



# Synthesis and characterization of Piperidine-4-carboxylic acid functionalized Fe<sub>3</sub>O<sub>4</sub> nanoparticles as a magnetic catalyst for Knoevenagel reaction

E. Karaoğlu<sup>a</sup>, A. Baykal<sup>a,\*</sup>, M. Şenel<sup>a</sup>, H. Sözeri<sup>b</sup>, M.S. Toprak<sup>c</sup>

<sup>a</sup> Department of Chemistry, Fatih University, 34500 B. Cekmece, Istanbul, Turkey

<sup>b</sup> TUBITAK-UME, National Metrology Institute, Gebze, 41470 Kocaeli, Turkey

<sup>c</sup> Division of Functional Materials, KTH-Royal Institute of Technology, 16440 Stockholm, Sweden

## ARTICLE INFO

### Article history:

Received 11 January 2012

Received in revised form 26 April 2012

Accepted 15 May 2012

Available online 24 May 2012

### Keywords:

- A. Magnetic materials
- B. Chemical synthesis
- C. X-ray diffraction
- D. Catalytic properties
- D. Magnetic properties

## ABSTRACT

Piperidine-4-carboxylic acid (PPCA) functionalized Fe<sub>3</sub>O<sub>4</sub> nanoparticles as a novel organic–inorganic hybrid heterogeneous catalyst was fabricated and characterized by XRD, FT-IR, TGA, TEM and VSM techniques. Composition was determined as Fe<sub>3</sub>O<sub>4</sub>, while particles were observed to have spherical morphology. Size estimations using X-ray line profile fitting (10 nm), TEM (11 nm) and magnetization fitting (9 nm) agree well, revealing nearly single crystalline character of Fe<sub>3</sub>O<sub>4</sub> nanoparticles. Magnetization measurements reveal that PPCA functionalized Fe<sub>3</sub>O<sub>4</sub> NPs have superparamagnetic features, namely immeasurable coercivity and absence of saturation. Small coercivity is established at low temperatures. The catalytic activity of Fe<sub>3</sub>O<sub>4</sub>–PPCA was probed through one-pot synthesis of nitro alkenes through Knoevenagel reaction in CH<sub>2</sub>Cl<sub>2</sub> at room temperature. The heterogeneous catalyst showed very high conversion rates (97%) and could be recovered easily and reused many times without significant loss of its catalytic activity.

Crown Copyright © 2012 Published by Elsevier Ltd. All rights reserved.

## 1. Introduction

Magnetic nanoparticles (MNPs) have attracted great interest because of their multifunctional physical and chemical properties. MNPs have high specific surface area that will be beneficial for a variety of applications, including ion exchange separation, drug delivery systems, magnetic resonance imaging, targeted gene therapy and biosensors. To enhance their performance in existing applications and to explore novel applications, understanding and controlling the effects of surface functional groups on magnetic nanospheres have become increasingly important issues for their applications [1–6].

In modern chemical research, catalysts and catalytic reactions are always attracting considerable attention in fundamental research and industrial applications [1–5]. Conventionally, heterogeneous catalysis is favored over homogeneous catalysis due to its ease of handling and regenerability [7–12]. PP (piperidine) was selected due to its catalytic activity particularly for Knoevenagel type of reactions such as mentioned in this work [13–15]. Because the presence of delocalized pi electrons on nitrogen in piperidine is responsible for the catalytic activity of PPCA for nitro-aldol reaction. This catalyst was selected to functionalize with Fe<sub>3</sub>O<sub>4</sub> due to magnetic decantation and reuse. Naked Fe<sub>3</sub>O<sub>4</sub> NPs have no considerable catalytic activity for nitro-aldol reaction.

The use of these MNP catalysts can address the isolation and recycling problem encountered in many heterogeneous and homogeneous catalytic reactions. Most importantly, the MNPs-supported catalysts show not only high catalytic activity but also a high degree of chemical stability and they do not swell in organic solvents [16–18]. MNP catalysts can be recovered with an external magnetic field and their catalytic efficiency remains after many repeated reactions [19].

In this study, we describe the preparation of (Piperidine-4-carboxylic acid) Fe<sub>3</sub>O<sub>4</sub>–PPCA nanocatalyst with high magnetic sensitivity and application in Knoevenagel reaction. Fe<sub>3</sub>O<sub>4</sub> nanoparticles were synthesized through a co-precipitation method [4] and surface modified with (Piperidine-4-carboxylic acid) PPCA.

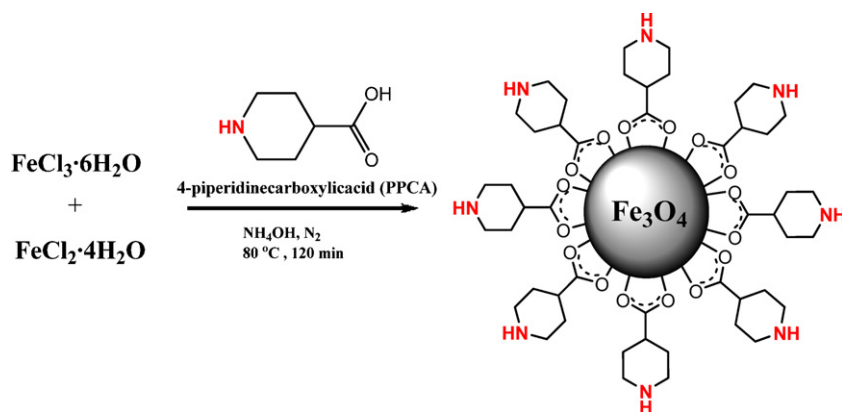
To the best of our knowledge, this is the first report on the preparation of Piperidine-4-carboxylic acid coated Fe<sub>3</sub>O<sub>4</sub> nanocatalyst material. Its magnetic and catalytic properties were evaluated and detailed results are presented. Finally, the catalytic behavior of Fe<sub>3</sub>O<sub>4</sub>–PPCA nanoparticles was measured by the Knoevenagel reaction.

## 2. Experimental

### 2.1. Chemicals and Instrumentation

4-Piperidinecarboxylic acid (PPCA), FeCl<sub>3</sub>·6H<sub>2</sub>O, FeCl<sub>2</sub>·4H<sub>2</sub>O, nitroethane (NE), acetaldehyde (A1), heptanal (A2), benzaldehyde

\* Corresponding author. Tel.: +90 212 866 33 00x2060; fax: +90 212 866 34 02.  
E-mail address: [hbaykal@fatih.edu.tr](mailto:hbaykal@fatih.edu.tr) (A. Baykal).



**Scheme 1.** Preparation of  $\text{Fe}_3\text{O}_4$ -PPCA nanoparticles.

(**A3**) and  $\text{NH}_3(\text{aq})$  (Merck) were used as-received, without further purification.

X-ray powder diffraction (XRD) analysis was conducted on a Rigaku Smart Lab Diffractometer operated at 40 kV and 35 mA using  $\text{Cu K}\alpha$  radiation.

Fourier transform infrared (FT-IR) spectra were recorded in transmission mode with a Perkin Elmer BX FT-IR infrared spectrometer. The powder samples were ground with KBr and compressed into a pellet. FT-IR spectra in the range  $4000\text{--}400\text{ cm}^{-1}$  were recorded in order to investigate the nature of the chemical bonds formed.

Transmission electron microscopy (TEM) analysis was performed using a FEI Tecnai G2 Sphera microscope. A drop of diluted sample in alcohol was dripped on a TEM grid.

The thermal stability was determined by thermogravimetric analysis (TGA, Perkin Elmer Instruments model, STA 6000). The TGA thermograms were recorded for 5 mg of powder sample at a heating rate of  $10\text{ }^\circ\text{C}/\text{min}$  in the temperature range of  $30\text{--}800\text{ }^\circ\text{C}$  under nitrogen atmosphere.

VSM measurements were performed by using a SQUID magnetometer (Quantum Design MPMS XL). The magnetization measurements were carried out in an external field up to 15 kOe at several temperatures.

## 2.2. Procedure

### 2.2.1. Preparation of (Piperidine-4-carboxylic acid) $\text{Fe}_3\text{O}_4$ -PPCA nanoparticles

$\text{Fe(III)}$  and  $\text{Fe(II)}$  salts (with the molar ratio of 2:1) were dissolved in 100 mL deionized water and kept at a constant temperature of  $40\text{ }^\circ\text{C}$  for 15 min with vigorous stirring. Then a certain amount of PPCA and  $\text{NH}_4\text{OH}$  solution were added to the above mixture until the pH was raised to 11 at which a black suspension was formed. This suspension was then refluxed at  $100\text{ }^\circ\text{C}$  for 6 h, with vigorous stirring.  $\text{Fe}_3\text{O}_4$ -PPCA nanoparticles was separated from the aqueous solution by magnetic decantation, washed with distilled water several times and then dried in an

oven overnight (Scheme 1). Whole synthesis was done under  $\text{N}_2$  atmosphere.

### 2.2.2. General procedure for Knoevenagel reaction catalyzed by $\text{Fe}_3\text{O}_4$ -PPCA

In a typical Knoevenagel reaction the novel MNP supported nanoparticle catalyst, dichloromethane, acetaldehyde (**A1**) and nitroalkane were added into a round bottomed flask and stirred at  $80\text{--}100\text{ }^\circ\text{C}$  in Ar atmosphere for 2–3 h. After completion of the reaction, mixture was cooled to room temperature, the catalyst (MNPs) was recovered by external magnet and product (**P1**) was washed with ethanol and dried at  $80\text{ }^\circ\text{C}$  for 5 h (Scheme 2). Then same catalyst reaction was carried out with heptanal (**A2**) and benzyl aldehyde (**A3**) according to Scheme 2 and obtained products were assigned as (**P2**) and (**P3**) respectively.

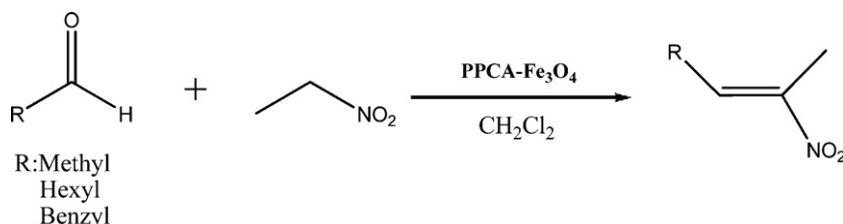
## 3. Results and discussion

### 3.1. XRD analysis

Phase investigation of the crystalline product was performed by XRD and the diffraction pattern is presented in Fig. 1. The XRD pattern indicates that the product consists of magnetite,  $\text{Fe}_3\text{O}_4$ , and the diffraction peaks are broadened owing to very small crystallite size. All of the observed diffraction peaks are indexed by the cubic structure of  $\text{Fe}_3\text{O}_4$  (JCPDS no. 19-629) revealing a high phase purity of magnetite. The following reaction is suggested for the formation of magnetite:



The mean size of the crystallites was estimated from the diffraction pattern by line profile fitting method using Eq. (1) given in Refs. [20,21]. The line profile, shown in Fig. 1 was fitted for observed six peaks with the following miller indices: (2 2 0), (3 1 1), (4 0 0), (4 2 2), (5 1 1), and (4 4 0). The average crystallite size,  $D$ , was obtained as  $10 \pm 0.1\text{ nm}$  as a result of this line profile fitting.



**Scheme 2.** Nitro-aldol condensation reaction.

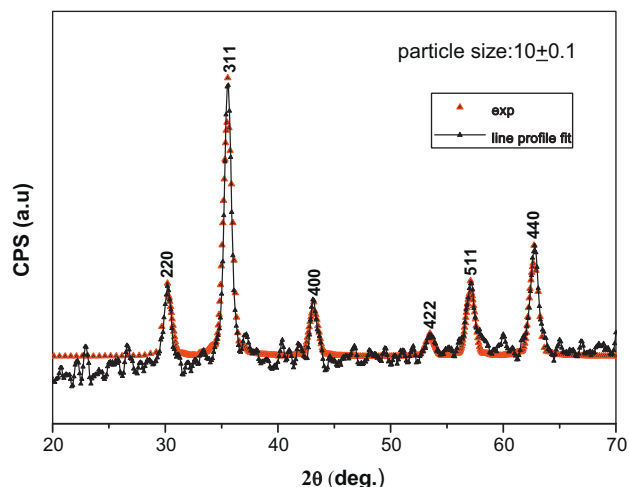


Fig. 1. XRD powder pattern of  $\text{Fe}_3\text{O}_4$ -PPCA nanoparticles.

### 3.2. FT-IR analysis

The FT-IR spectra of the PPCA,  $\text{Fe}_3\text{O}_4$  NPs and  $\text{Fe}_3\text{O}_4$ -PPCA nanoparticles are shown in Fig. 2. In the spectrum of  $\text{Fe}_3\text{O}_4$ -PPCA the intense peak at  $1590\text{ cm}^{-1}$  was derived from the existence of the C=O stretch. The surfactant molecules in the adsorbed state were subjected to the solid surface. As a result, the characteristic bands shifted to a lower frequency region, which indicated that the hydrocarbon chains in the monolayer surrounding the nanoparticles were in a closed-packed, crystalline state [22]. It is worth to note that the C=O stretch band of the carboxyl group, which was present at  $1650\text{ cm}^{-1}$  in the spectrum (PPCA), but it is absent in the spectrum for  $\text{Fe}_3\text{O}_4$ -PPCA. Two new bands appeared at  $1525$  and  $1590\text{ cm}^{-1}$ , which were ascribed to asymmetric  $\nu_{\text{as}}(\text{COO}^-)$  and symmetric  $\nu_{\text{s}}(\text{COO}^-)$  stretch of carboxyl group. This result can be explained that the bonding pattern of the carboxylic acids on the surface of  $\text{Fe}_3\text{O}_4$  nanoparticles was a combination of molecules bonded symmetrically and molecules bonded at an angle to the surface [23–27]. These results revealed that PPCA were chemisorbed onto the  $\text{Fe}_3\text{O}_4$  NPs as a carboxylate. The interaction between the carboxylate head and the metal atom was categorized as four types: monodentate, bridging (bidentate), chelating (bidentate), and ionic interaction [22,28,29]. According to Zhang

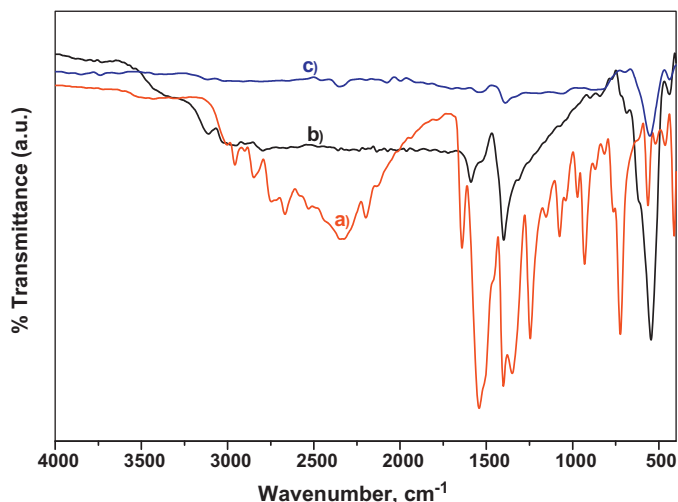


Fig. 2. FT-IR spectra of (a) PPCA, (b)  $\text{Fe}_3\text{O}_4$ -PPCA and (c) bulk  $\text{Fe}_3\text{O}_4$ .

et al. the wave number separation,  $D$ , between the  $\nu_{\text{as}}(\text{COO}^-)$  and  $\nu_{\text{s}}(\text{COO}^-)$  IR bands can be used to distinguish the type of the interaction between the carboxylate head and the metal atom. The largest  $D$  ( $200\text{--}320\text{ cm}^{-1}$ ) was corresponding to the monodentate interaction and the smallest  $D$  ( $<110\text{ cm}^{-1}$ ) was for the chelating bidentate. The medium range  $D$  ( $140\text{--}190\text{ cm}^{-1}$ ) was for the bridging bidentate [30]. In this study, the  $D$  ( $1590 - 1525 = 65\text{ cm}^{-1}$ ) was ascribed to chelating bidentate, where the interaction between the  $\text{COO}^-$  group and the Fe atom was covalent (Fig. 2b). [16] The inorganic lattice vibration for  $\text{Fe}_3\text{O}_4$  appears in the range  $400\text{--}700\text{ cm}^{-1}$  (Fig. 2a). As prepared powder presents characteristic peaks that are exhibited by the commercial magnetite powder: metal–oxygen band,  $\nu_1$ , observed at  $590\text{ cm}^{-1}$  corresponds to intrinsic stretching vibrations of the metal at tetrahedral site ( $\text{Fe}_{\text{tetra}} \rightarrow \text{O}$ ), whereas metal–oxygen band observed at  $445\text{ cm}^{-1}$ ;  $\nu_2$ , is assigned to octahedral–metal stretching ( $\text{Fe}_{\text{octa}} \rightarrow \text{O}$ ) [23–26,28].

### 3.3. TG analysis

Thermal stability of  $\text{Fe}_3\text{O}_4$ , PPCA and  $\text{Fe}_3\text{O}_4$ -PPCA nanoparticles was analyzed by TGA and thermograms are presented in Fig. 3a, b, c respectively. PPCA shows three-step weight loss behavior (Fig. 3c). The initial weight loss up to  $100\text{ }^\circ\text{C}$  is due to residual water; second step involves the decomposition of PPCA which started after  $250\text{ }^\circ\text{C}$  and continued up to  $300\text{ }^\circ\text{C}$ . The last step can be observed between  $400\text{ }^\circ\text{C}$  and  $450\text{ }^\circ\text{C}$  with 5% weight loss approximately. PPCA- $\text{Fe}_3\text{O}_4$  nanoparticles undergo similar decomposition steps as that of PPCA, but it has somehow greater stability due to interaction between PPCA and  $\text{Fe}_3\text{O}_4$ . Based on the thermograms given in Fig. 3, the percentages of organic (PPCA) and inorganic ( $\text{Fe}_3\text{O}_4$ ) in product are 20% and 80% respectively.

### 3.4. TEM analysis

Morphology of synthesized of  $\text{Fe}_3\text{O}_4$ -PPCA nanoparticles were investigated by TEM and few micrographs along with the size distribution diagram obtained thereof are presented in Fig. 4. Particles are observed to have spherical morphology from Fig. 4a and b. Average particle size is estimated as  $11.2 \pm 0.3\text{ nm}$  from the TEM micrographs (Fig. 4c), which is in a very good agreement with the crystallite size estimated from XRD as  $10 \pm 0.1\text{ nm}$ . This is an indication of nearly single crystalline character of  $\text{Fe}_3\text{O}_4$ -PPCA nanoparticles.

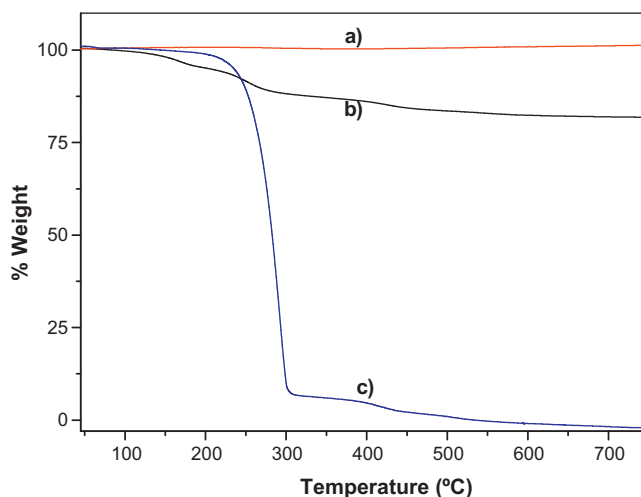


Fig. 3. TG thermograms of (a) uncoated  $\text{Fe}_3\text{O}_4$ , (b)  $\text{Fe}_3\text{O}_4$ -PPCA nanoparticles and (c) PPCA.

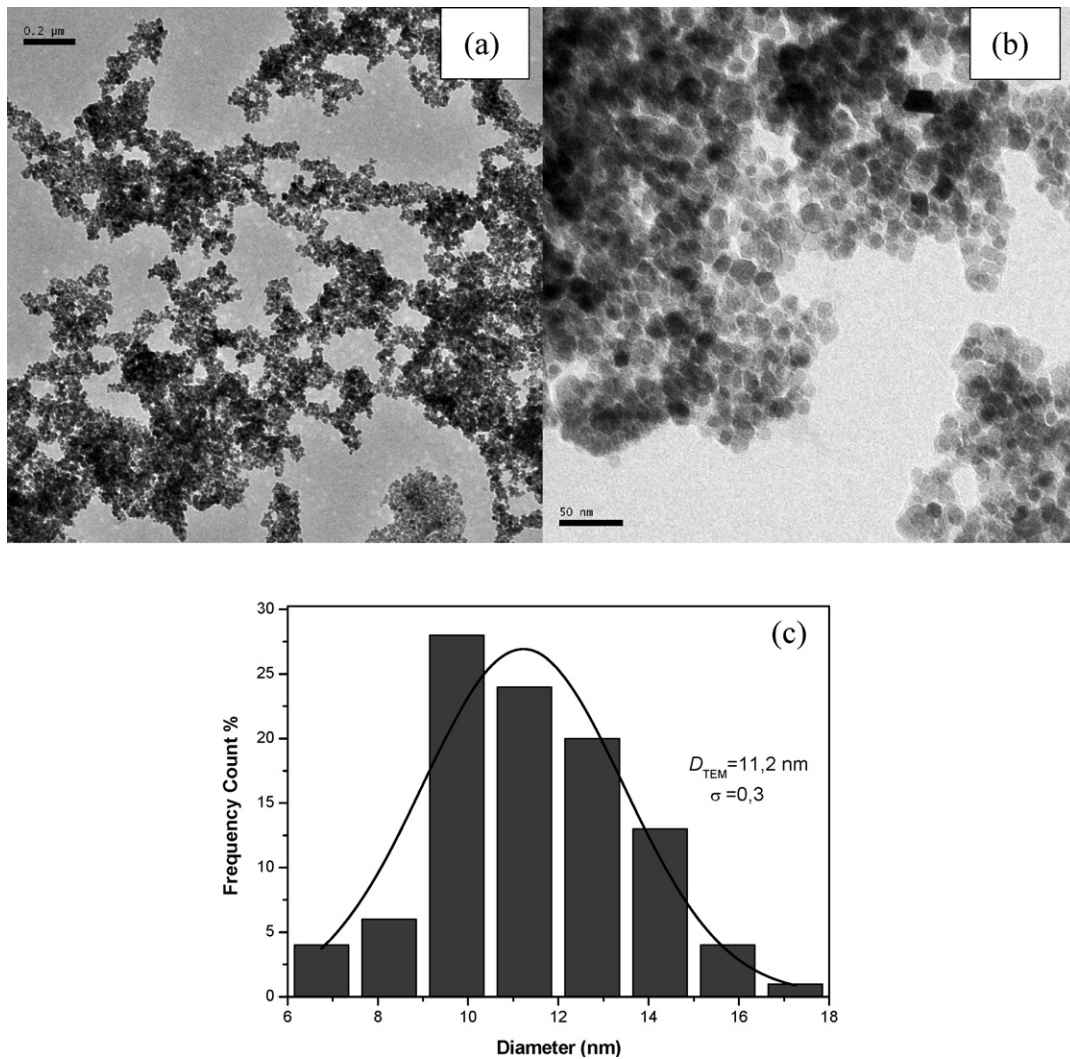


Fig. 4. (a and b) TEM micrographs of  $\text{Fe}_3\text{O}_4$ -PPCA nanoparticles with different magnifications; (c) size distribution histogram obtained from the TEM micrographs.

### 3.5. Magnetic characterization

Magnetization curves of  $\text{Fe}_3\text{O}_4$ -PPCA NPs measured at different temperatures from 10 K to room temperature and up to external field of 15 kOe are shown in Fig. 5. At 300 K, M–H hysteresis curve has an immeasurable coercivity and remanence. In addition, magnetization of the samples increases with external magnetic field without reaching to a saturation even at 1.5 T. These are characteristic features of the super-paramagnetic (SP) nanoparticles. Specific saturation magnetization of the sample is 60 emu/g at 15 kOe. However, this value should be normalized to the weight of the magnetic core, which is about 80% of the total. Then,  $M_s$  of the  $\text{Fe}_3\text{O}_4$  NPs becomes 72 emu/g that is still far from the theoretically predicted value (i.e., 92 emu/g). The possible reason in nanoparticle systems is the difference in spin ordering at the surface of particles over that in the bulk, setting up a magnetic core-shell configuration. Surface effects dominates the properties of the nanoparticles since decreasing the particle size increases the surface to core spin ratio. Surface effects results from the lack of translational symmetry at the boundaries of the particle due to the lower coordination number and existence of broken magnetic exchange bonds which lead to the surface spin disorder and frustration. Hence, reduced  $M_s$  can be ascribed to surface spin disorder and canting [31,32]. As temperature decreases down to

50 K and 10 K, small coercivity of nearly 200 and 130 Oe was established, respectively.

Magnetization of superparamagnetic particles can be described by the Langevin function (Eq. (1)) which can be used to determine the particle size.

$$M = M_s \left\{ \coth\left(\frac{\mu H}{k_B T}\right) - \frac{k_B T}{\mu H} \right\} \quad (1)$$

here,  $\mu$  denotes the mean magnetic moment of a single particle,  $H$  is applied field and  $k_B T$  corresponds to the thermal energy of the particles. The Langevin relation considers the each particle as a magnetic monodomain. The relationship, Eq. (2), between the mean magnetic moment of a particle and saturation magnetization of system of particles can be used to calculate average magnetic particle size,  $D$ .

$$\mu = \frac{M_s \pi \rho D^3}{6} \quad (2)$$

where  $\rho$  is the density of the sample.

Mean magnetic moment, which is used as a fitting parameter, is determined by fitting Eq. (1) to M–H hysteresis curve of the n nanoparticles that is normalized to the bulk mass, as  $14,206 \mu_B$  at 300 K. Then, using this value, mean magnetic particle size is found as

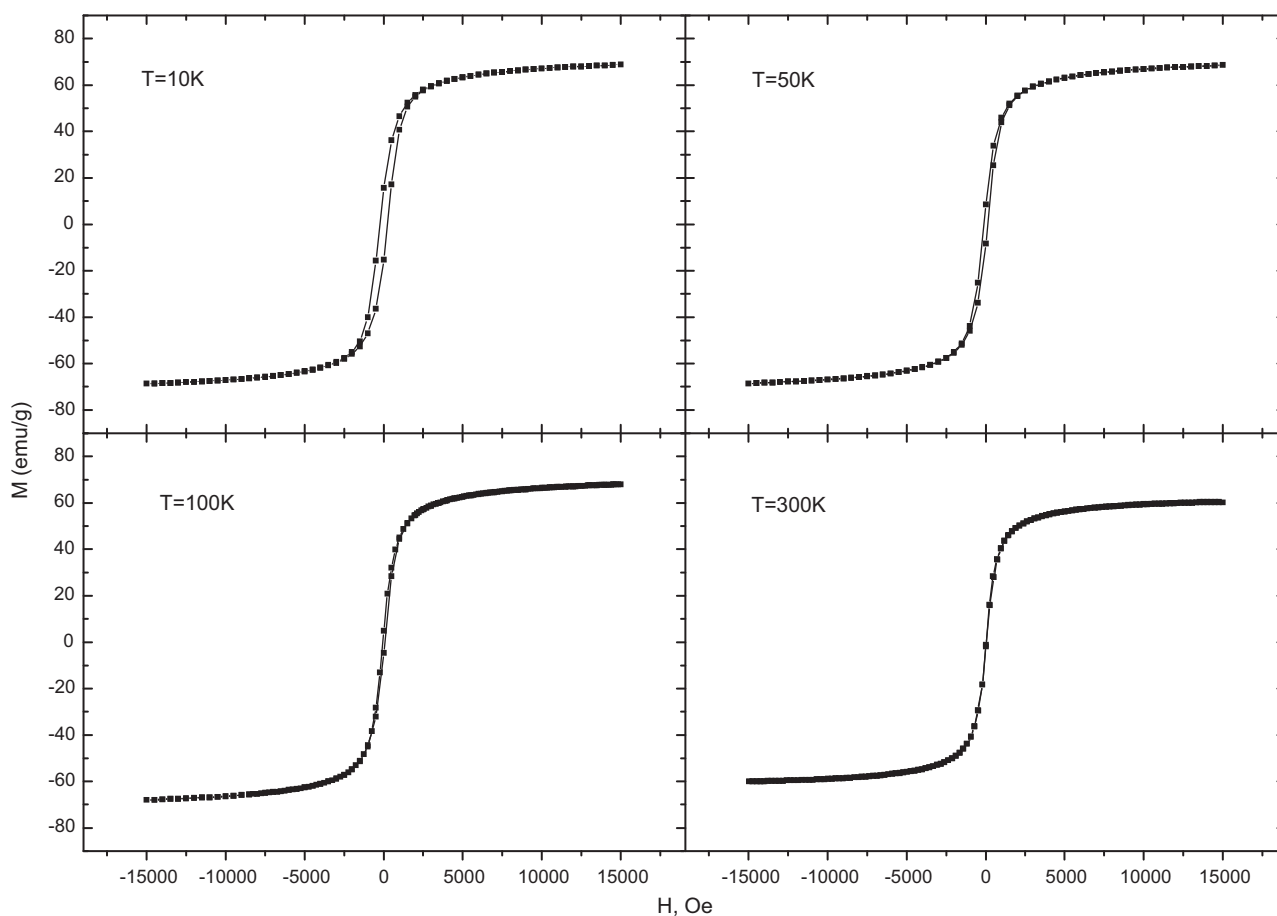


Fig. 5. M–H hysteresis curves of  $\text{Fe}_3\text{O}_4$ -PPCA nanoparticles at various temperatures.

$8.7 \pm 1.0$  nm. This number is slightly smaller than the particle size values obtained from X-ray line profile fitting ( $10 \pm 0.1$  nm) and TEM ( $11.2 \pm 0.3$ ) estimations due to the exclusion of magnetically dead layer in magnetic size estimation. The relationship between these values is an indication of each nanoparticle being a single magnetic domain.

### 3.6. Catalytic activity of $\text{Fe}_3\text{O}_4$ -PPCA

The Knoevenagel reaction is a famous and widely used synthetic pathway for carbon-carbon bond formation reaction in organic synthesis. The catalytic performance of the  $\text{Fe}_3\text{O}_4$ -PPCA NPs for Knoevenagel reaction was evaluated for the synthesis of Synthesis of Nitro Alkenes. To evaluate the efficiency of the Knoevenagel reaction by nanocatalyst, FT-IR spectrum of the reactants and products were studied and are presented in Fig. 6.

Table 1

Catalytic activity of  $\text{Fe}_3\text{O}_4$ -PPCA NPs for the synthesis of nitro alkenes (0.5 g catalyst, 25 °C, in  $\text{CH}_2\text{Cl}_2$ ).

Reactants	Conversion <sup>a</sup> (%)	Yield <sup>b</sup> (%)
<b><math>\text{Fe}_3\text{O}_4</math>-PPCA nanocatalyst</b>		
A1 + NE	~99	~92
A2 + NE	~77	~67
A3 + NE	~67	~60
<b>Naked <math>\text{Fe}_3\text{O}_4</math> nanoparticles</b>		
A1 + NE	~6	~4
A2 + NE	~4	~3
A3 + NE	~3	~2

<sup>a</sup> Determined by  $^{13}\text{C}$  NMR.

<sup>b</sup> Yield of isolated product.

The characteristic carbonyl stretching of aldehyde reactants can be seen at  $1725\text{ cm}^{-1}$ . The O=C stretch of the alpha, beta-unsaturated compound – benzaldehyde – is at a lower wavenumber (can be seen at  $1700\text{ cm}^{-1}$ ) than that of the saturated aliphatic aldehydes. As it can be seen from the FT-IR spectra of the products in Fig. 6, peak of the carbonyl group disappeared after catalytic reaction. The peak at  $1678\text{ cm}^{-1}$  at the FT-IR spectrum of the products belongs to C=C double bond. The results are listed in Table 1, which reveal that all reactants were converted to products effectively. The catalytic activity of naked  $\text{Fe}_3\text{O}_4$  and  $\text{Fe}_3\text{O}_4$ -PPCA was compared to show the catalytic selectivity of PPCA for Knoevenagel reaction in Table 1. The results show that the catalytic activity of the naked  $\text{Fe}_3\text{O}_4$  is considerably lower than the  $\text{Fe}_3\text{O}_4$ -PPCA.

The Knoevenagel reaction is a famous and widely used synthetic pathway for carbon-carbon bond formation reaction in organic synthesis [33,34]. There are few recent reports on the use of heterogeneous catalysts for Knoevenagel reaction [35,36]. The use of MNPs is advantageous as compared to other heterogeneous catalytic methods due to their ease of separation from the reaction medium. Functionalized MNPs were used by few researchers for Knoevenagel reaction [36–40].

As it has been found, the selectivity to the Knoevenagel product is >99% so are conversions and the yields of product. As expected for nucleophilic addition reactions with complete conversion being achieved for A1. The obtained conversion of A2 and A3 were remarkably lower than the A1 meant that the type of the aldehyde chain effect the conversion of the products due to steric effect of bulky group. The PPCA coated magnetic nanoparticle catalyst was easily separated from the reaction mixture by magnetic decantation after the reaction.

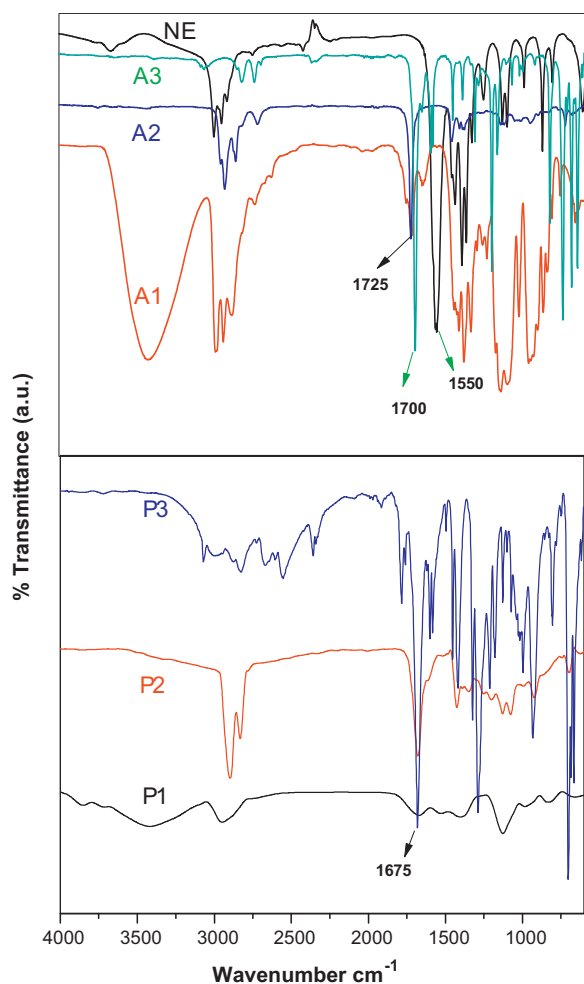


Fig. 6. FT-IR spectra of reactants of synthesis of nitro alkenes (A1, A2, A3 and NE) and products (P1, P2 and P3).

The key feature of the magnetically separable catalysis is the reusability of catalyst. The reusability of the catalyst was examined by carrying out repeated runs on the same batch of the used 0.5 g magnetic catalyst in Knoevenagel reaction of A1 and NE. As shown in Fig. 7, the catalytic activity of the magnetic catalyst did not decrease significantly even after four catalytic cycles and the

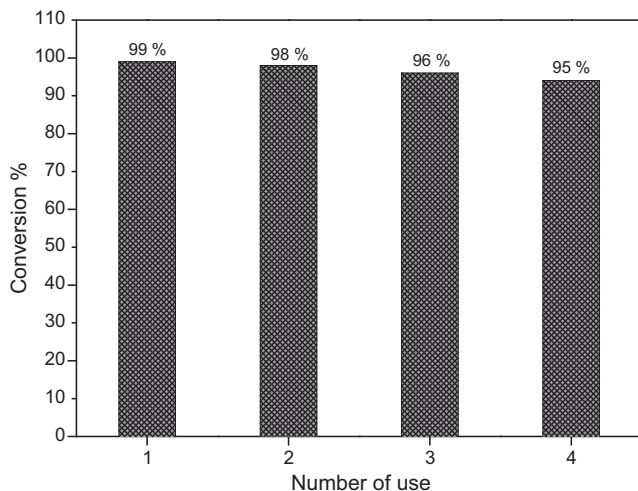


Fig. 7. Reusability of the magnetic catalyst for Knoevenagel reaction of A1 + NE.

catalyst could be completely recovered with external magnetic field. Which indicates that the magnetic catalyst is suitable for recyclable heterogeneous catalysis applications.

#### 4. Conclusion

We report for the first time on a novel one-pot reflux route for the fabrication of Piperidine-4-carboxylic acid (PPCA) functionalized  $\text{Fe}_3\text{O}_4$  nanoparticles as a novel organic-inorganic hybrid heterogeneous catalyst. Size evaluation via various techniques revealed size of  $\text{Fe}_3\text{O}_4$  particles around 10–11 nm with nearly single crystalline character. Magnetization measurements showed that  $\text{Fe}_3\text{O}_4$ -PPCA catalyst has a no coercivity and remanence together with unsaturated magnetization at high field.  $\text{Fe}_3\text{O}_4$ -PPCA catalyst possesses a high saturation magnetization (60 emu/g) and it is recoverable by magnetic decantation and could be reused several times without significant loss in catalytic activity and selectivity for Knoevenagel reaction. Our method has the advantage that no further modification of the magnetic particles is necessary for utilization as catalyst. Further studies on the effects of  $\text{Fe}_3\text{O}_4$ -PPCA catalyst on the catalytic activity for other catalyst systems are in progress.

#### Acknowledgements

The authors are thankful to the Fatih University, Research Project Foundation (Contract no: P50020902-2).

#### References

- [1] Y. Tai, L. Wang, G. Yan, J. Gao, H. Yua, L. Zhang, *Polym. Int.* 60 (2011) 976–994.
- [2] A. Afkhami, R. Norooz-Asl, *Colloids Surf. A* 346 (2009) 52–57.
- [3] A. Ito, H. Jitsunobu, Y. Kawabe, H. Ijima, M. Kamihira, *Tissue Eng. C* 15 (2009) 413–423.
- [4] J. Zhang, R.D.K. Misra, *Acta Biomater.* 3 (2007) 838–850.
- [5] J.L. Zhang, R.S. Srivastava, R.D.K. Misra, *Langmuir* 23 (2007) 6342–6351.
- [6] E. Taboada, R. Solanas, E. Rodriguez, R. Weissleder, A. Roig, *Adv. Funct. Mater.* 19 (2009) 2319–2324.
- [7] M. Mingliang, Q. Zhang, D. Yin, J. Dou, H. Zhang, H. Xu, *Catal. Commun.* 17 (2012) 168–172.
- [8] Y. He, C. Cai, *Catal. Commun.* 12 (2010) 678–683.
- [9] X. Zhang, A. Liu, W. Chen, *Org. Lett.* 10 (2008) 3849–3852.
- [10] Y. Gao, C. Chen, H. Gau, J. Bailey, E. Akhadov, D. Williams, H. Wang, *Chem. Mater.* 20 (2008) 2839–2844.
- [11] T. Mishra, *Catal. Commun.* 9 (2008) 21–26.
- [12] W. Li, J. Liu, C. Yan, *Carbon* 49 (2011) 3463–3470.
- [13] S. Fioravanti, L. Pellacani, P.A. Tardella, M.C. Vergari, *Org. Lett.* 10 (2008) 1449.
- [14] J. Simpson, D.L. Rathbone, D.C. Billington, *Tetrahedron Lett.* 40 (1999) 7031.
- [15] J.K. Augustine, Y.A. Naik, A.B. Mandal, N. Chowdappa, V.B. Praveen, *J. Org. Chem.* 72 (2007) 9854.
- [16] K.K. Senapati, S. Roy, C. Borgohain, P. Phukan, *J. Mol. Catal. A: Chem.* 352 (2012) 128–134.
- [17] D. Lee, J. Lee, H. Lee, S. Jin, T. Hyeon, B.M. Kim, *Adv. Synth. Catal.* 348 (2006) 41.
- [18] R. Abu-Resiz, H. Alper, D. Wang, M.L. Post, *J. Am. Chem. Soc.* 128 (2006) 5279.
- [19] E. Karaoğlu, A. Baykal, H. Erdem, L. Alpsoy, H. Sözeri, *J. Alloys Compd.* 509 (2011) 9218.
- [20] T. Wejrzanowski, R. Pielaszek, A. Opalińska, H. Matysiak, W. Lojkowski, K.J. Kurzydowski, *Appl. Surf. Sci.* 253 (2006) 204.
- [21] R. Pielaszek, in: *Proceedings of the XIX Conference, Krakow, Poland, Appl. Crystallogr.* 2003, p. 43.
- [22] K. Nakamoto, *Infrared and Raman Spectra of Inorganic and Coordination Compounds*, John Wiley & Son, New York, 1997.
- [23] B. Ünal, M.S. Toprak, Z. Durmus, H. Sözeri, A. Baykal, *J. Nanopart. Res.* 12 (2010) 3057.
- [24] B. Ünal, Z. Durmus, A. Baykal, H. Sözeri, M.S. Toprak, L. Alpsoy, *J. Alloys Compd.* 505 (2010) 172.
- [25] Z. Durmus, H. Kavas, A. Baykal, H. Sözeri, L. Alpsoy, S.Ü.C. elik, M.S. Toprak, *J. Alloys Compd.* 509 (2011) 2555.
- [26] B. Ünal, Z. Durmus, H. Kavas, A. Baykal, M.S. Toprak, *Mater. Chem. Phys.* 123 (2010) 184.
- [27] Y.T. Tao, *J. Am. Chem. Soc.* 115 (1993) 4350.
- [28] T. Özkaya, M.S. Toprak, A. Baykal, H. Kavas, Y. Köseoğlu, B. Aktaş, *J. Alloys Compd.* 472 (2009) 18.
- [29] Y. Ren, K. Iimura, T. Kato, *Langmuir* 17 (2001) 2688.
- [30] L. Zhang, R. He, H.C. Gu, *Appl. Surf. Sci.* 253 (2006) 2611.
- [31] R.H. Kodama, A.E. Berkowitz, E.J. McNiff, S. Foner, *Phys. Rev. Lett.* 77 (2) (1996) 394.

- [32] X. Batlle, A. Labarta, *J. Phys. D: Appl. Phys.* 35 (2002) R15–R42.
- [33] E. Knoevenagel, *Berichte* 31 (1898) 2585.
- [34] K.K. Senapati, C. Borgohain, P. Phukan, *J. Mol. Catal. A* 339 (2011) 24.
- [35] V.S.R. Rajasekhar Pullabhotla, A. Rahman, S.B. Jonnalagadda, *Catal. Commun.* 10 (2009) 365.
- [36] J.M. Khurana, K. Vij, *Catal. Lett.* 138 (2010) 104.
- [37] N.T.S. Phan, C.W. Jones, *J. Mol. Catal. A: Chem.* 253 (2006) 123.
- [38] Y. Zhang, Y. Zhao, C. Xia, *J. Mol. Catal. A: Chem.* 306 (2009) 107.
- [39] Y. Zhang, C. Xia, *Appl. Catal. A: Gen.* 366 (2009) 141.
- [40] C.S. Gill, W. Long, C.W. Jones, *Catal. Lett.* 131 (2009) 425.